

Cyclic load testing and numerical modeling of concrete columns with substandard seismic details

Mohammad S. Marefat[†], Mohammad Khanmohammadi[‡],
Mohammad K. Bahrani^{††}, and Ali Goli^{‡‡}

*Department of Civil Engineering, University of Tehran, Tehran, PO. Box 11365-4563, Iran
(Received April 20, 2005, Accepted September 23, 2005)*

Abstract. Recent earthquakes have shown that many of existing buildings in Iran sustain heavy damage due to defective seismic details. To assess vulnerability of one common type of buildings, which consists of low rise framed concrete structures, three defective and three standard columns have been tested under reversed cyclic load. The substandard specimens suffered in average 37% loss of strength and 45% loss of energy dissipation capacity relative to standard specimens, and this was mainly due to less lateral and longitudinal reinforcement and insufficient sectional dimensions. A relationship has been developed to introduce variation of plastic length under increasing displacement amplitude. At ultimate state, the length of plastic hinge is almost equal to full depth of section. Using calibrated hysteresis models, the response of different specimens under two earthquakes has been analyzed. The analysis indicated that the ratio between displacement demand and capacity of standard specimens is about unity and that of deficient ones is about 1.7.

Keywords: reinforced concrete column; defective seismic details; cyclic load test; plastic hinge length; numerical modeling.

1. Introduction

Recent earthquakes have shown that many of existing buildings in Iran sustain heavy damage due to defective seismic details. One common type of existing buildings consists of five story rigid frame concrete structures. To assess vulnerability of this type of buildings against earthquake, a test program has been conducted at structural laboratory of University of Tehran.

There are numerous reports of cyclic and shaking table test of columns, beams, and joints in the technical literature (e.g. Esmaeily, *et al.* 2004, Hashem, *et al.* 2003, Pujol, *et al.* 2002, Eberhard, *et al.* 2002, Brachman 2002, Paultre, *et al.* 2001, Mo & Wang 2000, Xiao and Martirosyan 1998, Ono *et al.* 1989, Saatcioglu and Ozcebe 1989, Otani and Sozen 1972, Celebi and Penzien 1973). The results of such studies have led to available codes and regulations. Most of such tests have been conducted under circumstances different from those of countries like Iran, and specific conditions of local constructions such as concrete quality, member and section dimensions, amount and arrangement of reinforcement, and site seismic demand, justify a separate study. The results of a

[†] Dean and Associate Professor, Corresponding Author, E-mail: mmarefat@ut.ac.ir.

[‡] Ph.D. Candidate of Structural Engineering, E-mail: mkhan394@yahoo.com

^{††} MSc Student of Earthquake Engineering, E-mail: bahrani_mk@yahoo.com

^{‡‡} MSc Student of Structural Engineering, E-mail: goli_eng@yahoo.com

study that has been conducted under local conditions are discussed here.

1.1. Specification of specimens

To design the test specimens, a reference frame has been defined on the basis of average characteristics of existing buildings (Fig. 1). Once again, the frame has been designed according to ACI318-99, seismic provisions of intermediate ductility which is commonly used in Iran, to define a standard frame. Therefore two types of specimens have been designed: substandard and standard. Both frames had similar span lengths and column heights, and both were subjected to identical seismic demand. In total, six specimens have been tested, three columns with defective seismic details, i.e., NBCM-11, NBCC-12, NTCM-14, and three others with standard characteristics, i.e., SBCC-7, SBCM-8, STCM-9. The scale of specimens was 1:2 in dimension and their height was 750 mm, and axial load was proportioned to position of each column in the building. Table 1 shows characteristics of reinforcement, and Table 2 presents specifications of specimens and axial load ratio. Arrangement of reinforcement and sectional view are given in Fig. 2 and Fig. 3. It is seen that the defective specimens have smaller sectional area, lower lateral and longitudinal reinforcement ratios by an average values of 17%, 38%, and 20%, respectively, relative to standard ones. Since two types of columns are subject to identical seismic demand in the reference frame, the differences may characterize deficiency of substandard columns.

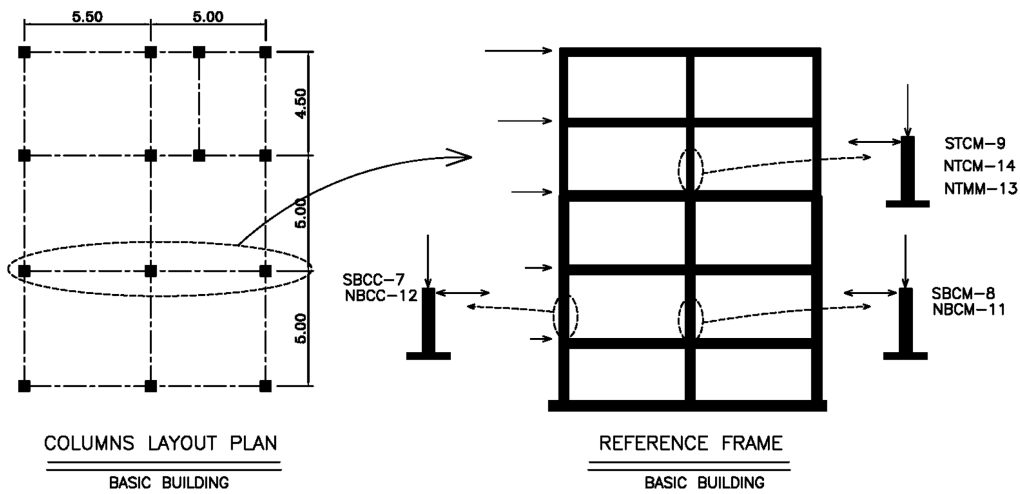


Fig. 1 Plan of basic building and view of reference frame

Table 1 Characteristics of reinforcements

Reinforcement type	Ultimate strain	Ultimate stress (MPa)	Modulus of elasticity (GPa)	Yield strain	Yield stress (MPa)
Longitudinal	0.18	670	200	0.002	393
Stirrups	0.25	290	185	0.0012	220

1.2. Test setup and load pattern

The test setup is shown in Fig. 4. A horizontal hydraulic actuator, with a capacity of 100 kN,

Table 2 Summary of test results and specifications of specimens

Specimen	Substandard			Standard		
	NTCM-14	NBCC-12	NBCM-11	STCM-9	SBCM-8	SBCC-7
Longitudinal reinforcement ratio ρ_s (%)	2.8	2.5	2.26	2.0	3.0	3.0
Lateral reinforcement volumetric ratio ρ_v (%)	0.60	0.66	0.88	1.2	1.1	1.1
Confinement index k^*	1.50	1.40	1.65	1.58	1.45	1.48
Cross-section dimensions $b \times h$ (mm ²)	150×150	200×150	200×200	175×175	200×200	200×200
Area $A=b \times h$ (mm ²)	22500	30000	40000	30625	40000	40000
f'_c (MPa)	20.1	25.2	24.5	24.0	28.0	27.0
$P/A_g f'_c$	0.31	0.23	0.25	0.19	0.22	0.16
Yield Drift (%)	1.00	0.83	0.76	0.76	0.78	0.87
H_{max}	22.4	28.9	59.4	31.1	78.3	60.1
$H_{max}/(bd \sqrt{f'_c})$	4.0	3.2	4.7	3.9	5.3	4.2
Displacement Ductility	3.1	5.9	8.0	4.8	7.3	6.9
Work-Damage Index, ω	12.9	43.5	99.8	38.4	127.1	195.5

*based on relationship proposed by Paulay and Priestly (1992).

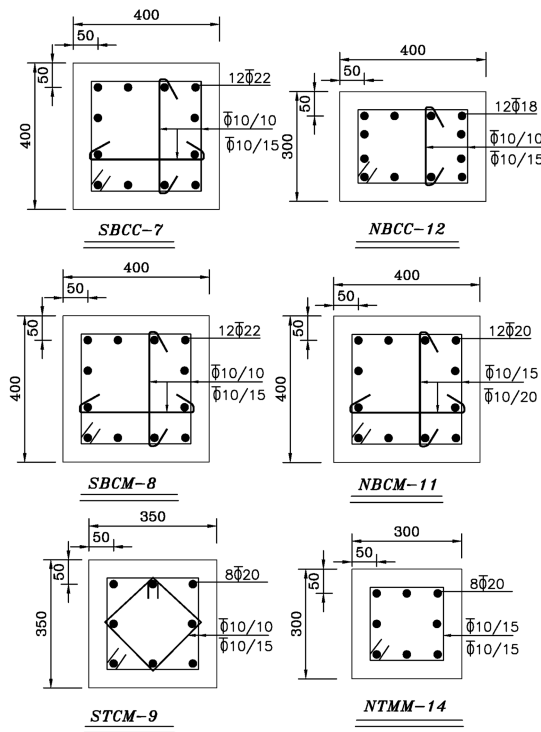


Fig. 2 Sectional view of columns of reference frame

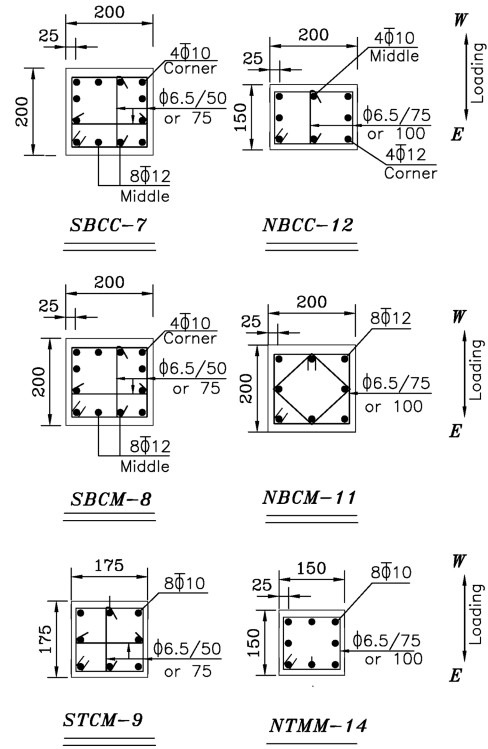


Fig. 3 Sectional view of test specimens

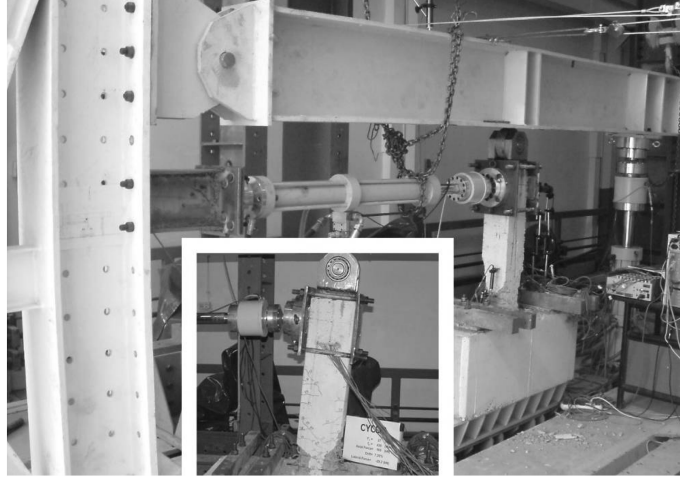


Fig. 4 A view of test setup

applies load to the free end of the specimen in two opposite directions. A vertical 250 kN actuator applies constant axial load to the columns. Loads are measured by load cells which are built in the actuators, and several LVDTs record horizontal and vertical displacement at critical sections. Several strain gauges are attached to longitudinal and transverse bars, at different levels of specimens, to record magnitude of strain at different stages. Horizontal loading has been applied in stroke control mode, in a quasi-static manner, and follows an increasing triple cycle amplitude pattern. Vertical axial load has been kept constant during the tests, in force control mode.

2. Test results

2.1. Lateral force-lateral displacement relationship

The relationship between lateral drift and lateral force, and the effect of $P-\Delta$, of different specimens is shown in Fig. 5. Important stages including first yield of reinforcement, yield of member, cracking, spalling, and buckling of bars are also included.

Fig. 5(a) illustrates hysteresis curve of Specimen NBCM-11 that shows a symmetric shape and a gradual reduction of strength caused by $P-\Delta$ effect. The response is almost ductile such that final stage, 20% loss of strength, is reached at a drift ratio of 6%. Fig. 5(b) illustrates the response of Specimen NBCC-12 with a symmetric shape without considerable ductility, relative to other substandard specimens. In comparison to previous specimen, both have almost identical axial load ratio, but because of reduction of confinement and lateral reinforcement in the latter, a relatively sudden drop of strength and stiffness is experienced. Fig. 5(c) shows the behavior of Specimen NTCM-14. The ratio of ductility is relatively small and 20% of the strength is lost at a drift ratio of only 3.5%. In addition, decline of in-cycle and out-cycle stiffness is larger than other substandard specimens.

Fig. 5(d) illustrates the behavior of Specimen SBCC-7 which may be characterized by a symmetric shape, a relatively large energy absorption capacity, and a relatively ductile form. In the

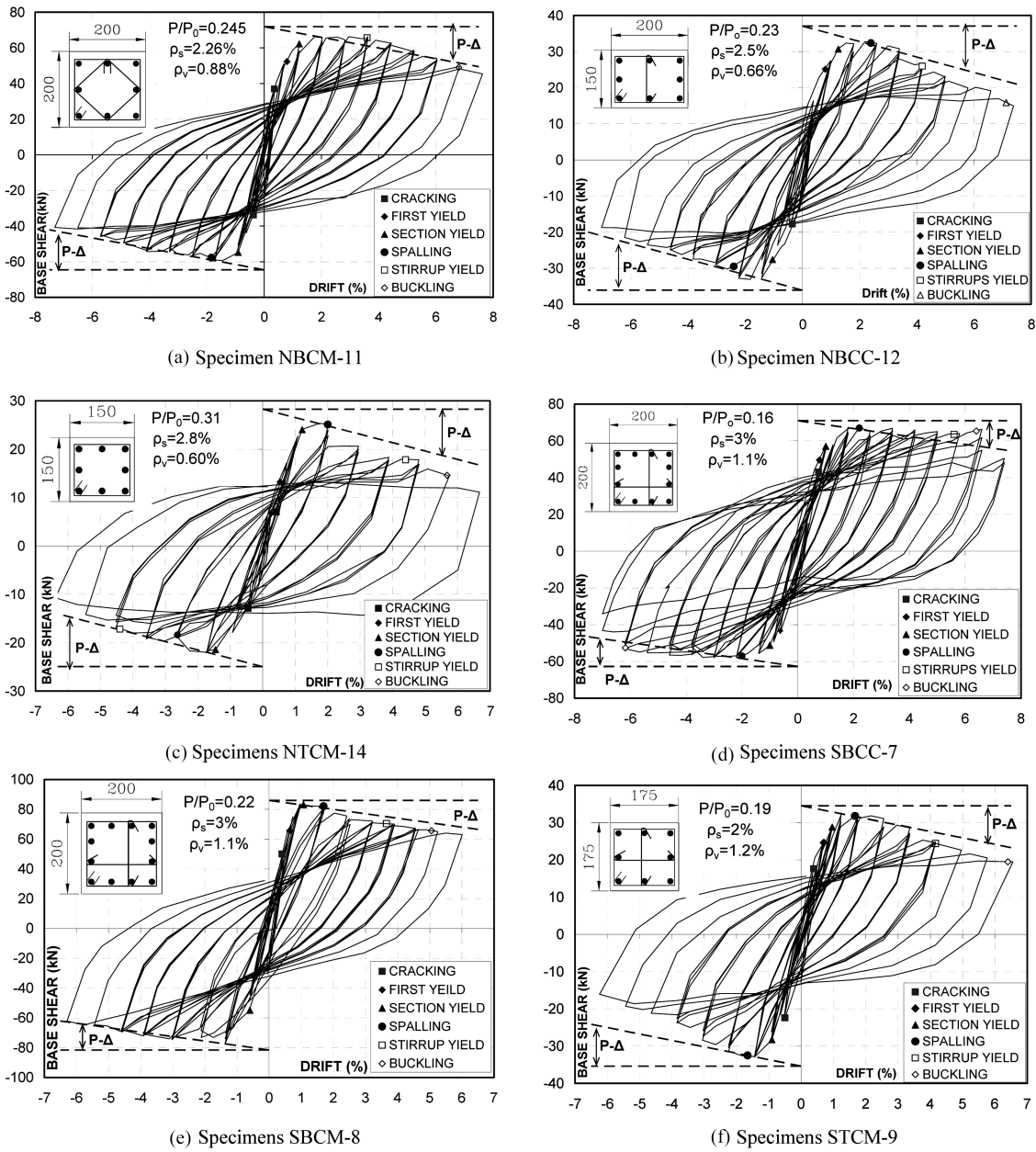


Fig. 5 Hysteresis curves of test specimens

non-linear phase, the strength has been preserved up to a drift of 6.5%. At this drift, sudden drop of resistance has been caused by buckling of longitudinal reinforcement. Fig. 5(e) shows the behavior of Specimen SBCC-8. Out-cycle decline of strength and stiffness has appeared after yield of member in a gradual manner and in proportion to effect of axial force. In Fig. 5(f), hysteresis curve of Specimen STCM-9 shows less ductility relative to other columns and 20% loss of strength is reached at a drift ratio of only 3.8%.

Table 3 Ratio of results of standard to substandard specimens

Results	Specimen	STCM-9/ NTCM-14	SBCM-8/ NBCM-11	SBCC-7/ NBCC-12
Ratio of H_{\max}		1.38	1.31	2.08
Ratio of $H_{\max}/(bd\sqrt{f'_c})$		0.76	1.03	1.04
Ratio of <i>Displacement Ductility</i>		1.55	0.91	1.17
Ratio of <i>Work-Damage Index, ω</i>		2.97	1.27	4.49

Important characteristics of different specimens are given in Table 2 and the standard and substandard specimens are compared in Table 3. Regardless of Specimen NBCM-11, with relatively good behavior, other substandard specimens suffer relatively highly reduced maximum strength and lower displacement ductility relative to the respective standard ones. It should be noted that despite comparable ductility in the standard and substandard Specimens, e.g., SBCC-7 and NBCC-12, the deficient columns suffer significant loss of energy dissipation capacity relative to standard specimens. This is discussed subsequently.

3. Energy dissipation capacity

Energy dissipation capacity constitutes an important characteristic of members under cyclic action and large deformation motion. To assess capacity of energy dissipation, a non-dimensional index of work-damage, ω , has been proposed by Ehsani and Wight (1990) and has been adopted by other researchers (Sheikh and Khoury 1993, Paultre, Legeron, and Mongeau 2001) for analysis of cyclic loading tests on columns. This index is defined as follows:

$$\omega = \frac{1}{H'_{\max} U_{y1}} \sum_i E_i \left(\frac{K_i}{K_y} \right) \left(\frac{\Delta U_i}{U_{y1}} \right)^2 \quad (1)$$

where H'_{\max} is maximum base shear, U_{y1} yield displacement, ΔU_i the average of absolute values of negative and positive amplitudes at each cycle, K_y yield stiffness and E_i the dissipated energy at each cycle.

The value of work-damage index of different specimens and the ratio of standard to substandard results have been calculated and presented in Table 2 and Table 3. Evidently, a larger value of the index means higher energy absorption capacity caused by preserving stiffness and strength at larger displacement amplitudes.

Comparing columns at identical positions in the reference frame, it is seen that the defective specimens especially in edge columns and top story columns show much smaller energy absorption capacity. The difference varies between 22 to 79% with an average value of 45%. This means that the substandard columns are much more vulnerable under seismic action and suffer greater loss of strength and stiffness than standard columns. In fact, because of reduced sectional area, the ratios of axial force and shear force increase. On the other hand, lower ratios of longitudinal reinforcement undermine strength of the specimens, and insufficient confinement reduces stability of the response after yielding. Combination of these factors has resulted in a relatively significant loss of seismic capacity of defective columns.

4. Hysteresis model of columns

Hysteresis models are used for numerical simulation of structural response under cyclic load. Several famous hysteresis models have been developed in the literature (e.g. Takeda, *et al.* 1970, Kent and Park 1973, Saiidi and Sozen 1979, Saatcioglu 1991, Stone and Taylor 1992). In this study, a modified shape of Park model which is included in IDARC software (Valles, *et al.* 1996) has been

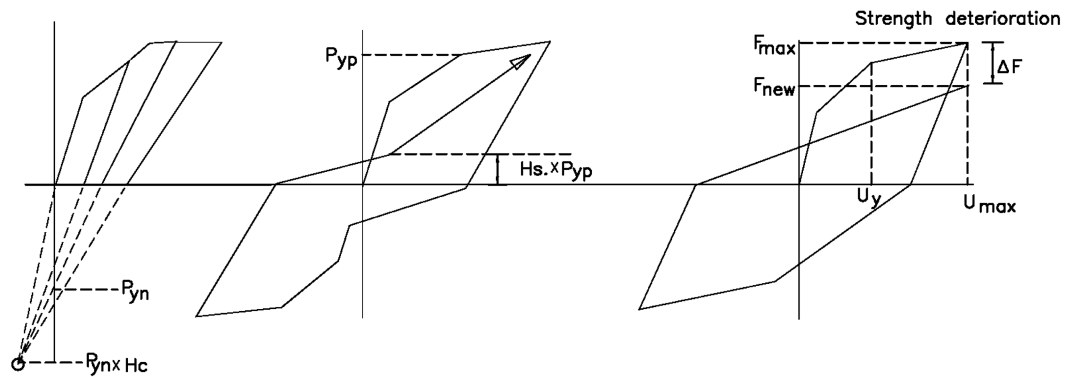


Fig. 6 Definition of parameters of modified hysteresis model of Park in IDARC (Valles, *et al.* 1996).

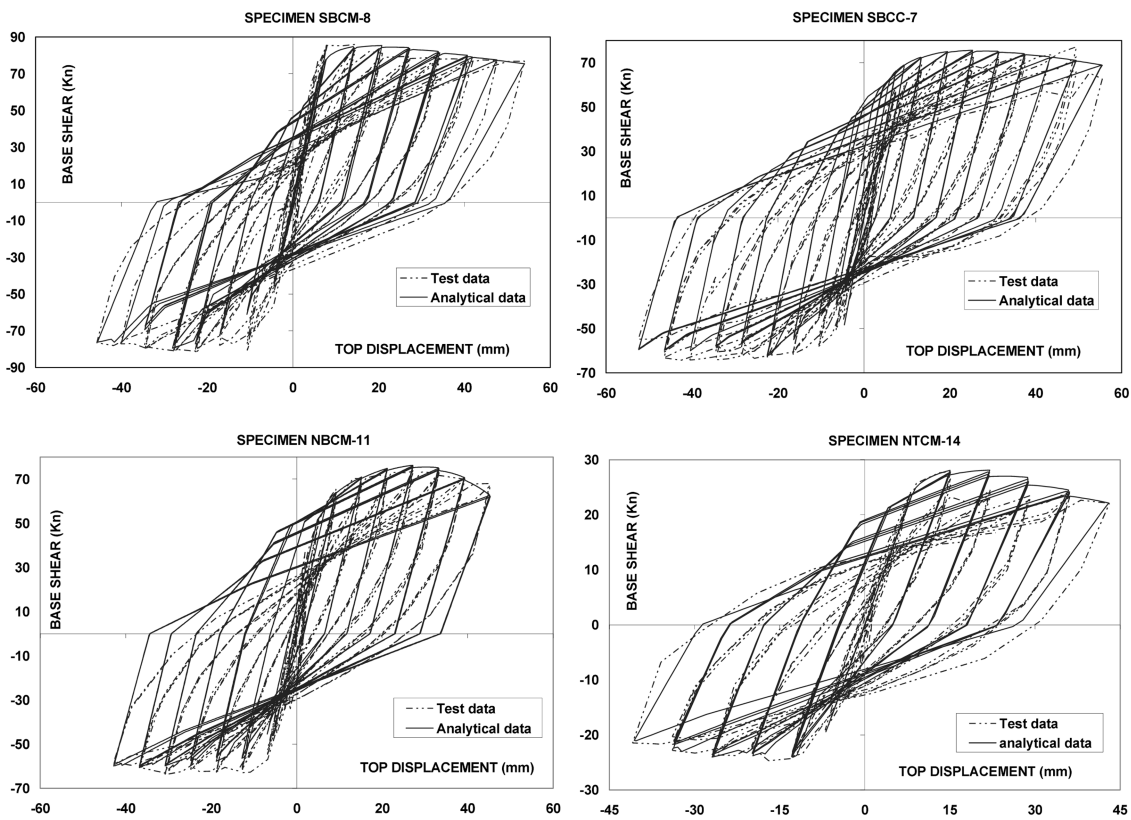


Fig. 7 Comparison between analysis and test results (without $P-\Delta$ effect)

used. In this model, a hysteresis response is defined by three main parameters, i.e., stiffness degradation, strength deterioration, and pinching effect. Fig. 6 illustrates these parameters.

In this model, deterioration of strength is related to energy and ductility as is described by Eq. (2).

$$F_{new} = F_{max} (1 - A_1 E - A_2 D) / F_y U_{ult} \tag{2}$$

where A_1 and A_2 account for in-cycle and out-cycle strength deterioration, respectively, F_y for yield strength, U_{ult} for ultimate displacement, E for energy of enclosed area of the curve, and D for ductility ratio. Parameters of F_{max} and F_{new} are described in Fig. 6.

For numerical simulation, characteristics of the specimens including backbone curve, curvature-moment relationship, cracking moment, yield moment, yield curvature, initial stiffness, post yield ratio, all in both positive and negative directions, have been introduced to the program. Hysteresis parameters consist of stiffness degradation, H_c , in-cycle strength degradation, A_1 , out-cycle strength degradation, A_2 , pinching effect, H_s , have been used as calibration factors. A relatively good agreement between test and analysis output is reached that may be seen in Fig. 7. The values of different parameters are given in Table 4.

Table 4 shows that the rate of stiffness degradation in unloading branch is the same for defective and standard specimens, as the respected parameter is equal to 40 for all specimens. Based on classification of Valles, *et al.* (1996), this value lies in the range of very little loss of stiffness, 15 to 200. But, in-cycle degradation of strength caused by energy dissipation, A_1 , of most substandard specimens is greater than that of standard ones. This lies in the range of very little, 0.01 to 0.08, for standard specimens, and lies in the range of moderate, 0.08 to 0.15, for substandard ones. The exception is Specimen NBCM-11 that shows good cyclic behavior that can be compared to the Standard Specimen SBCC-8. On the contrary, out-cycle degradation of strength caused by ductility,

Table 4 Values of different parameters for hysteresis models

Substandard		Standard		Specimen		Hysteresis Parameter
NTCM 14	NBCC 12	NBCM 11	STCM 9	SBCM 8	SBCC 7	
40	40	40	40	40	40	Unloading degradation stiffness (H_c)
0.10	0.10	0.03	0.06	0.05	0.02	In-cycle strength deterioration (A_1)
0.40	0.30	0.20	0.45	0.60	0.50	Out-cycle strength deterioration (A_2)
0.85	0.80	0.90	0.85	0.80	0.90	pinching effect (H_s)

Table 5 The results of time-history analysis of different specimens

Demand/ Capacity	Capacity based on test (mm)	Displacement demand (mm)		Characteristic Specimen
		Elcentro EQ.	Tabas EQ.	
0.935	44.9	25	42	SBCC-7
0.943	42.4	23	40	SBCM-8
1.16	30	27	35	STCM-9
0.886	44.9	19.7	39.8	NBCM-11
1.57	35.6	37	56.1	NBCC-12
2.63	23.4	33.2	61.6	NTCM-14

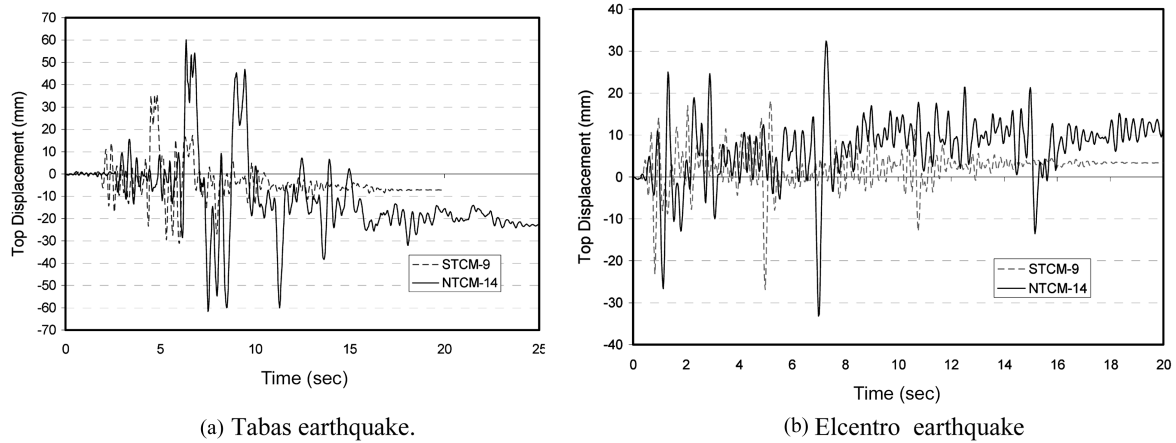


Fig. 8 The responses of specimens under Tabas and elcentro earthquakes

A_2 , of standard specimens is much greater than substandard ones. The effect of pinching of all specimens is quite small and is close to a limit value of $H_s=1$, e.g., without pinching. These parameters may be used for analyzing columns similar to those of the tests under earthquake motion.

Using calibrated hysteresis models, the response of different specimens under two earthquake records, Tabas north-south component and Elcentro east-west component, has been analyzed. The records have been preprocessed to account for scaling effects such as natural frequency, site effects, and expected yield base shear (Hashem, *et al.* 2003). Then, a non-linear time-history analysis has been carried out. The results of analysis have been given in Table 5, and the time-history responses of two specimens are illustrated in Fig. 8.

The maximum lateral displacements of different specimens, determined by dynamic time-history analysis, are presented in Table 5. Displacement capacity of different specimens is determined by tests and is assumed to be equal to displacement at a stage when 20% of maximum strength is lost. The first three specimens in the table are standard ones. For these specimens, the ratio between demand and capacity is about unity that means enough seismic capacity under respected earthquakes. The second three specimens are deficient columns for which the ratio between demand and capacity exceeds unity and reaches a value as large as 2.63 with an average value of 1.70. This means that the substandard specimens suffer relatively large loss of seismic capacity under the analyzed records of earthquakes.

5. Plastic hinge length

Under increasing lateral displacement, the expected plastic regions sustain relatively large strains and undergo non-linear behavior. Characteristics of non-linear region significantly influence the post-yield response of members. Based on theoretical and experimental studies, a number of equations have been developed to predict length of plastic hinge in flexural members by Zahn (1986), Priestley and Park (1987), Chai, *et al.* (1994), Corley (1966), Bayrak, *et al.* (2001), Esmaily, *et al.* (2004). A well-known and widely used equation is that presented by Priestly, *et al.* (1996) in the form of Eq. (3).

$$L_p = 0.08 L + 0.022 F_y d_b > 0.044 F_y d_b \text{ (mm, MPa)} \tag{3}$$

where L_p , L , F_y , d_b , are plastic hinge length, distance between maximum moment and contra-flexure point, yield stress of longitudinal bar, and diameter of longitudinal bar, respectively. Length of plastic hinge of different specimens, based on Eq. (3), is given in Table 6.

To evaluate plastic hinge length on the basis of test results, a uniform distribution of maximum curvature over an equivalent plastic length may be assumed. Then, the plastic length may be calculated using Eq. (4) (Paulay and Priestly 1992) as follows:

$$\Delta_p = (\varphi_u - \varphi_y) L_p (L - L_p/2) \tag{4}$$

where Δ_p , φ_y , φ_u , L_p , account for plastic lateral displacement, yield curvature, ultimate curvature, and plastic hinge length, respectively, where the first three parameters are measured in the tests. Based on test results, and using Eq. (4), the plastic hinge length of different specimens has been determined and given in Table 6.

The plastic hinge length determined by Eq. (3) and Eq. (4) assumes an equivalent length with a uniform distribution of plasticity. A distinction must be made between the equivalent plastic length and the region of plasticity. There is a growing gradient of strain under increasing amplitude of

Table 6 The ratio of plastic hinge length to sectional depth of different specimens

Calculation Method	NTCM	NBCC	NBCM	STCM	SBCM	SBCC
	14	12	11	9	8	7
Eq. (3) of Priestly (1996)	0.97	1.03	0.81	0.83	0.78	0.78
Based on length of damaged concrete	1.13	1.03	0.90	0.89	0.83	0.80
Based on Eq. (4) and test results	1.13	0.90	0.70	0.79	0.73	0.94
Based on records of curvature variation	1.44	1.28	1.03	1.11	1.19	1.04

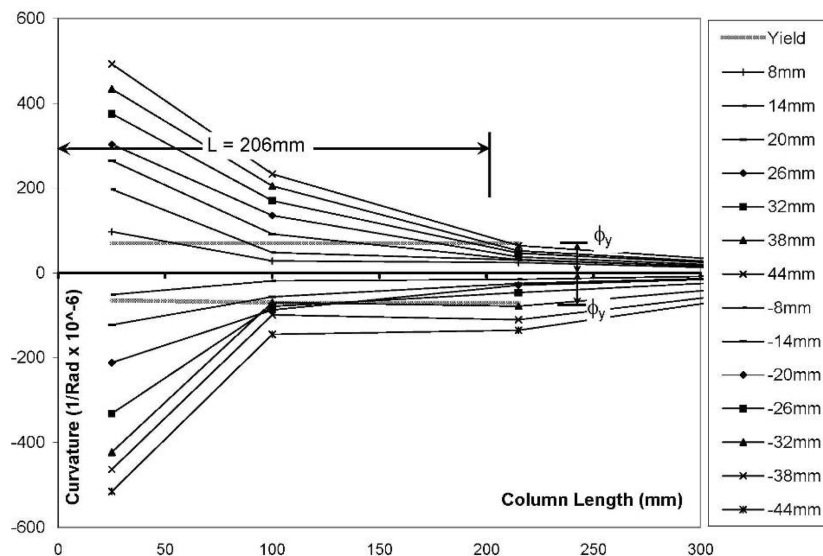


Fig. 9 Variation of sectional curvature for specimen NBCM-11

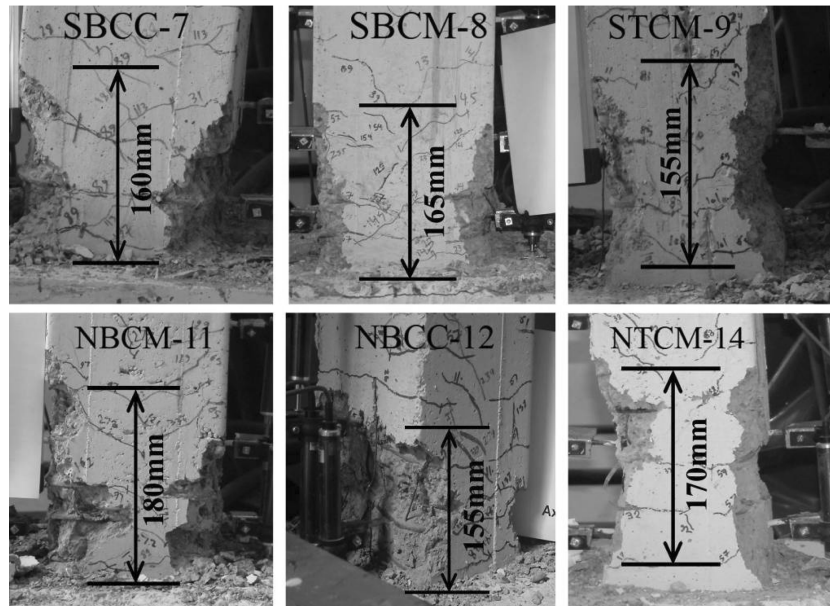


Fig. 10 Length of plastic hinge based on observation at the end of tests

deformation in the non-linear region. The maximum value of strain forms near the support and gradually decreases towards the opposite end of plastic region. In this study, variation of curvature over the expected length of plasticity has been recorded by means of several LVDTs that have been placed at three levels near the support, on both sides of specimens. The distance between first yield curvature and maximum curvature at the support is assumed to be equal to the plastic region (Paulay and Priestly 1992), (Ho and Pam 2003). For example, Fig. 9 illustrates variation of plastic length of Specimen NBCM-11 at successive steps. In this way, the length of plastic region for different specimens has been determined and presented in Table 6.

Visual inspection offers another way to estimate the length of plastic region. Since damage to concrete is mainly caused by large strains, the length of damaged area gives an indication of the length of plastic region. Based on judgment and visual inspection, the length of plastic hinge of different specimens has been estimated and given in Table 6. Fig. 10 illustrates the damaged area and the respected plastic hinge length of different specimens.

Table 6 shows that the first three methods have yielded comparable results for all specimens either substandard or standard, and the length of plastic hinge is about full depth of section. As is expected, the length of plastic region is always larger than the plastic hinge as is seen in the fourth row of Table 6. The difference between two lengths is, in average, about 35%. But, the plastic hinge length of Specimen NTCM-14 is greater than all other specimens and exceeds the depth of section. The main difference between this specimen and others relates to its axial force ratio that exceeds 30%. This is in harmony with the relationship developed by Zhan (1987), where the effect of axial force is described by a correction factor which is smaller than unity for axial force ratios smaller than 30%, and is greater than unity otherwise.

Another important issue is variation of plastic hinge length over the history of loading. The length of plastic hinge given in Table 6 is measured at ultimate state that normally defined as a state when 20% of the maximum strength is lost (Priestley and Seible and Calvi 1996). Fig. 9 shows that the

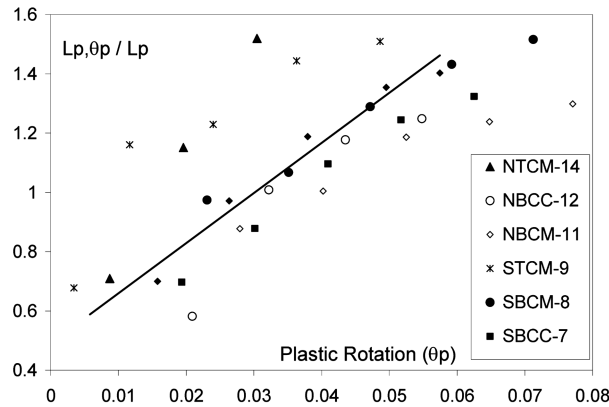


Fig. 11 Variation of plastic region length versus plastic rotation

length of non-linear region varies as lateral drift increases. This variation is especially important for non-linear analysis of structures. In this study, a relationship between plastic rotation and plastic region length has been developed.

Based on test data and by evaluating sectional curvature at different stages, the plastic region of various specimens is determined. The results are depicted in Fig. 11. A linear fit to the test data is drawn which forms the Eq. (5).

$$L_{p,\theta_p} = 0.75L_p (17\theta_p + 0.5) , \quad \theta_p > 0.01 \quad (5)$$

where L_p , $L_{p,\theta}$, θ_p are plastic hinge length, mm, according to Eq. (3), plastic hinge length, mm, based on tests, and plastic rotation, radian, respectively. As was mentioned, the plastic region is about 35% longer than the plastic hinge. Therefore, an equivalent plastic hinge length may be determined if the above equation is multiplied by 0.75.

Eq. (5) indicates that for plastic rotation of 0.05 radian, the plastic region is equal to L_p . Under expected seismic motions, a plastic rotation between 0.015 to 0.02 radians is anticipated [Englekirk 2003] which is about a half of the above rotation. Based on the above considerations, the plastic hinge length of columns under 0.015 to 0.02 radian of rotation is 0.5 to 0.6 times L_p . It follows that a plastic hinge length of about a half of depth of section can be expected under reference earthquakes.

6. Conclusions

To assess hysteretic response of concrete columns with substandard and standard seismic details, six columns have been tested under reversed cyclic load. Three specimens represent substandard buildings and three others represent well proportioned constructions, in accordance with provisions of intermediate ductility, ACI318-99. The respective standard and substandard columns were subject to identical seismic demand. The tests show that the defective columns suffer, in average, 37% loss of strength and 45% loss of energy dissipation capacity relative to standard specimens. This is mainly due to insufficient lateral and longitudinal reinforcement and smaller sectional area of substandard specimens relative to standard ones.

A relationship has been developed to introduce variation of plastic length under increasing displacement amplitude. The results indicated that, under axial load ratio less than 30% and at ultimate state, the length of plastic hinge is almost equal to full depth of section, and this does not depend on the type of specimen. But under expected seismic load, the length of plastic hinge is predicted to be about a half of depth of column. Using calibrated hysteresis models, the response of different specimens under two earthquakes has been analyzed. The analysis indicated that the ratio between displacement demand and capacity of standard specimens is about unity and that of deficient ones has an average value of 1.7. Based on test results, different parameters of hysteresis response and plastic hinge length for substandard and standard columns have been determined. These parameters can be used to simulate cyclic response of columns with characteristics similar to those of the tests.

Acknowledgements

The authors wish to express their appreciation to the authority of Deputy of Research of the University of Tehran, for financing this research work under project No. 614/4/883.

References

- Bayrak, O. and Sheikh, S. (2001), "Plastic hinge analysis", *J. Struct. Eng., ASCE*, September.
- Brachmann, I. (2002), "Drift limits of rectangular reinforced concrete columns subjected to cyclic loading" MS thesis, University of Kansas, Lawrence, Kans., Apr., 369.
- Celebi, M. and Penzien, J. (1973), "Experimental investigation into the seismic behavior of critical region of reinforced concrete components as influenced by moment and shear", Earthquake Eng. Res. Centre, Univ. of California, Berkeley, CA, EERC 73-4.
- Chai, Y. H., Priestley, M. J. N. and Seible, F. (1994), "Analytical model for steel jacketed RC circular bridge columns", *J. Struct. Eng., ASCE*, **120**.
- Corley, W. G. (1966), "Rational capacity of reinforced concrete beams", Bulletin D108, Skokie, Portland Cement Association, Research and Development Laboratories.
- Eberhard, M. (2002), "Reinforced concrete column test database", University of Washington, Seattle, Wash., www.ce.washington.edu/~peeral.
- Ehsani, M. R. and Wight, J. K. (1990), "Confinement steel requirements for connections in ductile frames," *J. Struc. Div., ASCE*, **116**(ST3), 751-767.
- Englekirk, R. E. (2003), *Seismic Design of Reinforced and Precast Concrete Buildings*, John Wiley and Sons, New York.
- Esmaily, A. and Xiao, Y. (2004), "Behavior of reinforced concrete columns under variable axial loading", *ACI Struct. J.*, **101**(1), Jan-Feb., 124-132.
- Hachem, M. M., Mahin, A. S. and Moehle, P. J. (2003), "Performance of circular reinforced concrete bridge columns under bidirectional earthquake loading", Pacific Earthquake Engineering Research Center, PEER2003/06.
- Ho, J. C. M. and Pam, H. J. (2003), "Inelastic design of low-axially loaded high-strength reinforced concrete columns", *J. Eng. Struct.*, **25**, 1083-1096.
- Kent, D. C. and Park, R. (1973), "Cyclic load behavior of reinforcing steel strain", *British Society for Strain Measurement*, **9**(3), 98-103.
- Lehman, D. E. and Moehle, P. J. (1998), "Seismic performance of well-confined concrete bridge columns", Pacific Earthquake Engineering Research Center, PEER1998/01.
- Mo, Y. L. and Wang, S. J. (2000), "Seismic behavior of rc columns with various tie configurations" *J. Struct. Eng., ASCE*, **126**(10), 279-313.

- Ono, A., Shirai, N., Adachi, H. and Sakamaki, Y. (1989), "Elasto-plastic behavior of reinforced concrete column with fluctuating axial force", *Transactions of the Japan Concrete Institute*, Vol. **11**, 239-246.
- Otani, S. and Sozen, M. A. (1972), "Behavior of multi-story reinforced concrete frames during earthquakes", Univ. of Illinois, Urbana, IL, Structural Research Series, No.392.
- Paulay, T. and Priestly, M. J. N. (1992), *Seismic Design of Reinforced Concrete and Masonry Buildings*, John Wiley and Sons, New York.
- Paultre, P., Legeron, F. and Mongeau, D. (2001), "Influence of concrete strength and transvers reinforcement yield strength on behavior of high-strength concrete columns", *ACI Struct. J.*, **98**(4), July-Aug., 490-501.
- Priestley, M. J. N and Park, R. (1987), "Strength and ductility of concrete bridge columns under seismic loading", *ACI Struct. J.*
- Priestley, M. J. N., Seible, F. and Calvi, G. (1996), *Seismic Design and Retrofit of Bridges*, John Wiley and Sons, New York.
- Pujol, S. (2002), "Drift capacity of reinforced concrete columns subjected to displacement reversals", Ph.D. Thesis, School of Civil Engineering, Purdue University.
- Saatcioglu, M. (1991), "Modeling hysteretic force-deformation relationships for reinforced concrete elements", *ACI*, SP127, 153-198.
- Saatcioglu, M. and Ozcebe, G. (1989), "Response of reinforced concrete columns to simulated seismic loading", *ACI Struct. J.*, January-February, 3-12.
- Saiidi, M. and Sozen M. A. (1979), "Simple and complex models for nonlinear seismic response of reinforced concrete structures", Civil Engineering Studies, University of Illinois, Structural Research Series No. 465.
- Sheikh, S. A. and Khoury, S. S. (1993), "Confined concrete columns with stubs", *ACI Struct. J.*, **90**(4), July-Aug., 414-431.
- Stone, W. C. and Taylor, A. W. (1992), "A predictive model for hysteretic failure parameters", *Proc. of Tenth World Conference on Earthquake Engrg.*, 2575-2580.
- Takeda, T., Sozen M. A. and Nielsen N. N. (1970), "Reinforced concrete response to simulated earthquakes", *J. Struc. Div., ASCE*, **96**(ST12), 2557- 2573.
- Valles, R. E., Reinhorn, M., Kunnath, S. K. and Li, C. (1996), "IDARC: A Program for inelastic damage analysis of buildings", Civil Engineering Studies, Technical Report NCEER-96-0010, State University of New York at Buffalo.
- Xiao, Y. and Martirosyan A. (1998), "Seismic performance of high strength concrete columns", *J. Struct. Eng., ASCE*, **124**(3), 241-251.
- Zahn, F. A. (1986), "Design of reinforced concrete bridge columns for strength and ductility", University of Canterbury, Department of Civil Engineering.